ELSEVIER

New Astronomy 1 (1996) 177–196

NEW ASTRONOMY

The HAWAII Infrared Detector Arrays: testing and astronomical characterization of prototype and science-grade devices

K.-W. Hodapp[a,1], J.L. Hora[a,2], D.N.B. Hall[a,3], L.L. Cowie[a,4], M. Metzger[a,5], E. Irwin[a,6], K. Vural[b,7], L.J. Kozlowski[b,8], S.A. Cabelli[b,9], C.Y. Chen[b,10], D.E. Cooper[b,11], G.L. Bostrup[b,12], R.B. Bailey[b,13], W.E. Kleinhans[c,14]

[a]*Institute for Astronomy, University of Hawaii, 2680 Woodlawn Drive, Honolulu, HI 96822, USA*[15]
[b]*Rockwell International Science Center, 1049 Camino dos Rios, Thousand Oaks, CA 91360, USA*[16]
[c]*Valley Oak Semiconductor, Westlake Village, CA 91362, USA*

Received 28 May 1996; accepted 4 July 1996
Communicated by Steven Beckwith

Abstract

Two generations of prototypes of a HgCdTe infrared detector array with 1024 × 1024 pixels developed by the Rockwell International Science Center have been tested in the new **Quick Infrared Camera**[17] (QUIRC) and an upgraded version of **KSPEC**[18], a cross-dispersed near-infrared spectrograph, on the University of Hawaii 2.2 m telescope.

The HAWAII (HgCdTe Astronomical Wide Area Infrared Imager) prototype devices achieved very good performance.

[1]E-mail: hodapp@uhifa.ifa.hawaii.edu; http://www.ifa.hawaii.edu/faculty/hodapp
[2]E-mail: hora@uhifa.ifa.hawaii.edu; http://www.ifa.hawaii.edu/faculty/hora
[3]E-mail: hall@uhifa.ifa.hawaii.edu
[4]E-mail: cowie@uhifa.ifa.hawaii.edu
[5]E-mail: metzger@uhifa.ifa.hawaii.edu
[6]E-mail: irwin@uhifa.ifa.hawaii.edu
[7]E-mail: kvural@scimail.risc.rockwell.com
[8]E-mail: sacabell@scimail.risc.rockwell.com
[9]E-mail: ljkozlow@scimail.remnet.rockwell.com
[10]E-mail: achen@scimail.remnet.rockwell.com
[11]E-mail: decooper@scimail.remnet.rockwell.com
[12]E-mail: glbostru@scimail.remnet.rockwell.com
[13]E-mail: rbbailey@scimail.remnet.rockwell.com
[14]E-mail: bill@valley-oak.com
[15]http://www.ifa.hawaii.edu
[16]http://www.risc.rockwell.com
[17]http://www.ifa.hawaii.edu/instrumentation/quirc/quirc.html
[18]http://www.ifa.hawaii.edu/instrumentation/kspec/kspec.html

PII S1384-1076(96)00013-9

The read-noise in correlated double sampling (CDS) is between 10 and 15 e^- rms, depending on the conditions of the operations and the way read-noise is computed. The quantum efficiency in H and K is above 50%. The full-well capacity is above 10^5 e^- at 0.5 V applied detector bias and is, in our system, limited by the dynamic range of the A/D converter. The residual excess dark-current problem known from NICMOS-3 devices (Hodapp et al., 1992) [PASP, 104, 441] is not fully resolved. However, it appears less serious in our first HAWAII prototype devices.

Using KSPEC, operation under low background conditions has been tested. At an operating temperature of 65 K, and using up to 128 samples of multi-sampling, a read-noise of < 5 e^- and a dark current < 1 e^-/min has been demonstrated. Tests of fast sub-array reads for wavefront sensing were conducted using QUIRC. For a sub-array frame repeat time of 11 ms, a read-noise of 6 e^- has been demonstrated.

An engineering-grade second-generation HAWAII device with reliable hybridization is now in routine operation in KSPEC. The first science-grade HAWAII device has now been installed in the QUIRC camera and is in routine operation.

PACS: 85.60.Bt; 95.55.Qf; 95.85.Jq
Keywords: Instrumentation: detectors; Instrumentation: spectrographs

1. Introduction

HgCdTe infrared detector arrays with a cutoff wavelength of 2.5 μm have found widespread use in ground-based astronomy, even though they were originally developed for space-based applications. The last generation of these arrays, the NICMOS-3 devices, were developed for the first infrared instrument to be installed in the Hubble Space Telescope (HST), the **Near Infrared Camera and Multi-Object Spectrograph**[19] (NICMOS) (Thompson 1994).

The reasons for choosing 2.5 μm HgCdTe for the HST instrument are the match of the cut-off wavelength to the onset of very strong thermal emission from a ≈ 300 K temperature telescope and the ease of cooling the detectors and the rest of the instrument to a temperature (around 77 K) where low background conditions can be achieved for these detectors. Exactly the same reasons make 2.5 μm HgCdTe an economical choice for a detector material for ground-based instruments.

Since the development of the NICMOS-3 detectors in 1989, the fabrication technology for hybrid HgCdTe devices has progressed from the 256×256 pixel format of those devices to routine fabrication of devices with a 640×480 format for some non-astronomical projects. The next step for astronomical detector arrays could therefore skip that format and go directly to a 1024×1024 format.

The main fabrication problem with large-format HgCdTe arrays is the thermal expansion mismatch between the multiplexer (silicon) and the detector array (PACE-1: HgCdTe on CdTe on sapphire). Even with detectors based on the PACE-1 process, however, the thermal mismatch can be mitigated by thinning the multiplexer and mounting the hybrid on a substrate that thermally matches the sapphire to reduce the mechanical stresses.

Based on this idea, the Rockwell International Science Center, under contract from the Institute for Astronomy (IfA) and with funding provided by the Air Force Phillips Laboratory, developed a new infrared detector array with a 1024×1024 pixel format. The multiplexer design was completed by the end of 1993, the first multiplexers were produced in March 1994, and the first fully functional prototype device was delivered to the IfA early in July 1994, in time for the first observing run with QUIRC during the comet Shoemaker-Levy 9 impact on Jupiter.

Laboratory characterization results for this first

[19] http://www.stsci.edu/ftp/instrument-news/NICMOS/topnicmos.html

generation of HAWAII devices were published by (Kozlowski et al. (1994)). A second engineering-grade device of this first generation was extensively tested in KSPEC under low background conditions between June and August 1995.

Subsequent work at Rockwell concentrated on the hybridization technology for these devices, to ensure their reliability over large numbers of thermocycles. Repeated thermocycling of test structures and second-generation engineering devices showed that the number of pixels lost (on average) in each thermocycle is small (10 to 20 pixels), albeit not zero.

This work resulted in a second-generation prototype device delivered to the IfA in August 1995. This device was used to upgrade KSPEC (Hodapp, 1994) for scientific use, after the laboratory tests mentioned above were completed.

The first science-grade HAWAII array was delivered in December 1995 and was used to upgrade QUIRC. This array was used for the tests of fast sub-array reads and is now being used routinely for scientific observations.

2. Basic characteristics of the HAWAII arrays

The HAWAII devices are laid out similarly to the NICMOS-3 devices in that they have four electrically independent quadrants, each quadrant reading out through one amplifier. In our system, a single read of the HAWAII array through four independent signal chains takes 2.7 s. Faster operation of the array is possible and we expect that with suitable read-out electronics, a single read could be completed in less than one second.

The unit cell of the HAWAII multiplexer (Fig. 1) contains only three field-effect transistors (FETs), rather than the four in NICMOS-3 multiplexers. The

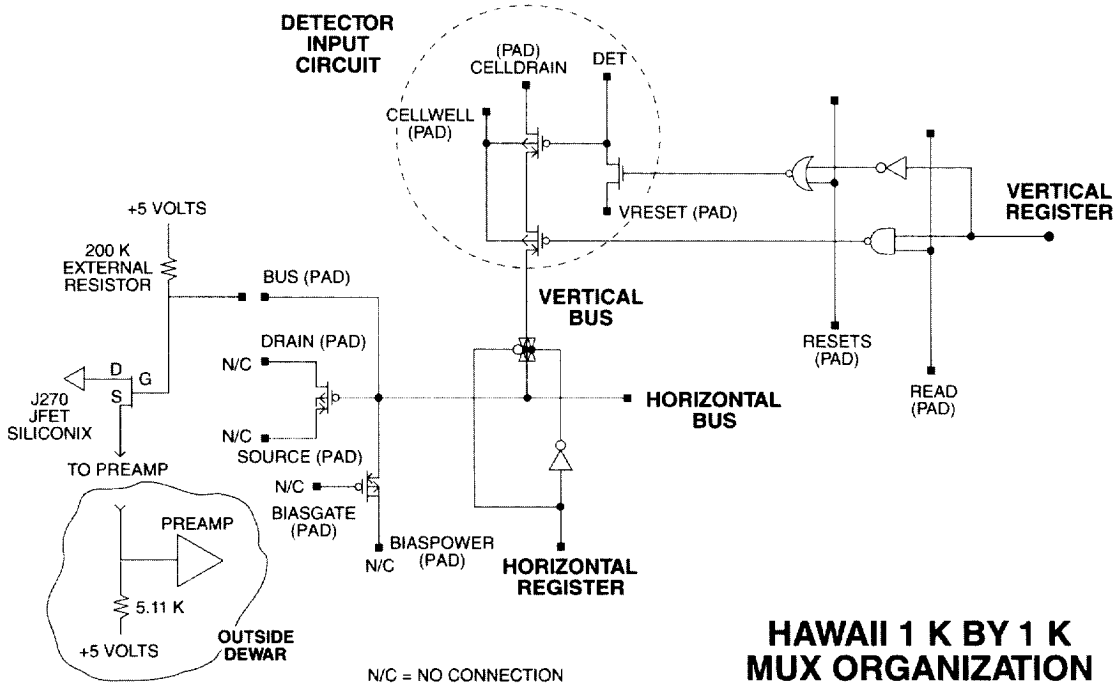

Fig. 1. Unit cell layout of the HAWAII devices.

FET allowing individual pixels to be reset has been eliminated, since read-out modes requiring that operation have been used only rarely and were not seen as an important scientific requirement. The HAWAII arrays are now designed to reset one row of pixels simultaneously. The new design of the reset circuit eliminates the charge redistribution effects commonly referred to as the reset anomaly, and thereby helps in the reduction of the read-noise.

Electroluminescence effects from the output amplifiers of the multiplexer have been a source of added photon flux in NICMOS-3 arrays, limiting the useful number of samples in multi-sampling read-out schemes that could be used to reduce noise. For operation under low-background conditions, we have provided the option to bypass the on-chip output amplifiers and to directly connect the bus to an external preamplifier stage, so that electroluminescence from the multiplexer can be minimized.

3. The infrared camera QUIRC

The acronym QUIRC (Quick Infrared Camera) describes the purpose and design philosophy of this system. The goal was to build a camera in a very short time (7 months) to keep up with Rockwell's aggressive development schedule for the HAWAII devices. The optical system in QUIRC (Fig. 2) is the one previously used in our NICMOS-3 camera (Hodapp et al., 1992) for 1:1 reimaging. Only the field lens needed to be changed to one with a higher index of refraction (ZnS), to keep spherical aberration in the pupil plane within acceptable limits. QUIRC is equipped with two filter wheels operated by cryogenic stepper motors. The zero position is encoded by a magnet installed on the filter wheel whose field is sensed by a Hall effect sensor.

Further, and different from the older camera, we installed a cryogenic pupil mask slide to adapt the camera to telescopes of different f-ratios without having to open the cryostat. This mechanism is driven by a stepper motor operated stainless steel lead screw, the nut is made out of MoS_2 impregnated Vespel.

The dewar is an up-looking design with a single large liquid nitrogen can (9 l volume) similar to that of the CCD dewars used at the IfA (Luppino & Miller, 1992). The dewar was designed for long periods of cold operation and has excellent vacuum stability; it has continuously operated for periods of more than 3 months without pumping. The cryogenic hold time is in excess of 24 hours.

The very first HAWAII devices produced by Rockwell were thermocycled a number of times during testing in their laboratory. In their test dewar, the hybrid device was thermally tightly coupled to the cryogen, and the cooldown time was short. Under those testing conditions, these early prototypes deteriorated rapidly from thermocycle to thermocycle, as expected from mechanical modelling of these hybrids.

Since we intended to use our engineering-grade device for astronomical observations for an extended period of time, we minimized the mechanical forces exerted by the device mount on the chip and increased the thermal resistance between the cold surface and the device, so that the device cooled down very slowly and ended up being operated at 96 K. This succeeded in avoiding rapid deterioration of our device, but led to a higher dark current (≈ 1 e^-/s) than was measured by Rockwell for the same device at 77 K operating temperature.

In this configuration QUIRC was used for 18 months for a wide variety of scientific projects (e.g., see (Hodapp & Ladd (1995)) for deep S(1) line imaging results). It was used at the UH 2.2 m telescope f/10 focus for wide-field imaging, at the f/31 focus for tip-tilt corrected imaging, at the Canada-France-Hawaii Telescope (CFHT) f/8 focus, and at the CFHT with the UH adaptive optics system (Roddier et al., 1994). Counting use at all telescopes, it was in astronomical operation for more than 50% of all nights. Fig. 3 shows a flatfield frame and Fig. 4 a typical science raw data frame taken with QUIRC and the engineering-grade HAWAII device.

In January 1996, QUIRC was upgraded with new detector electronics to allow faster read-out of the device through four parallel signal chains. Most importantly, the first HAWAII science-grade detector

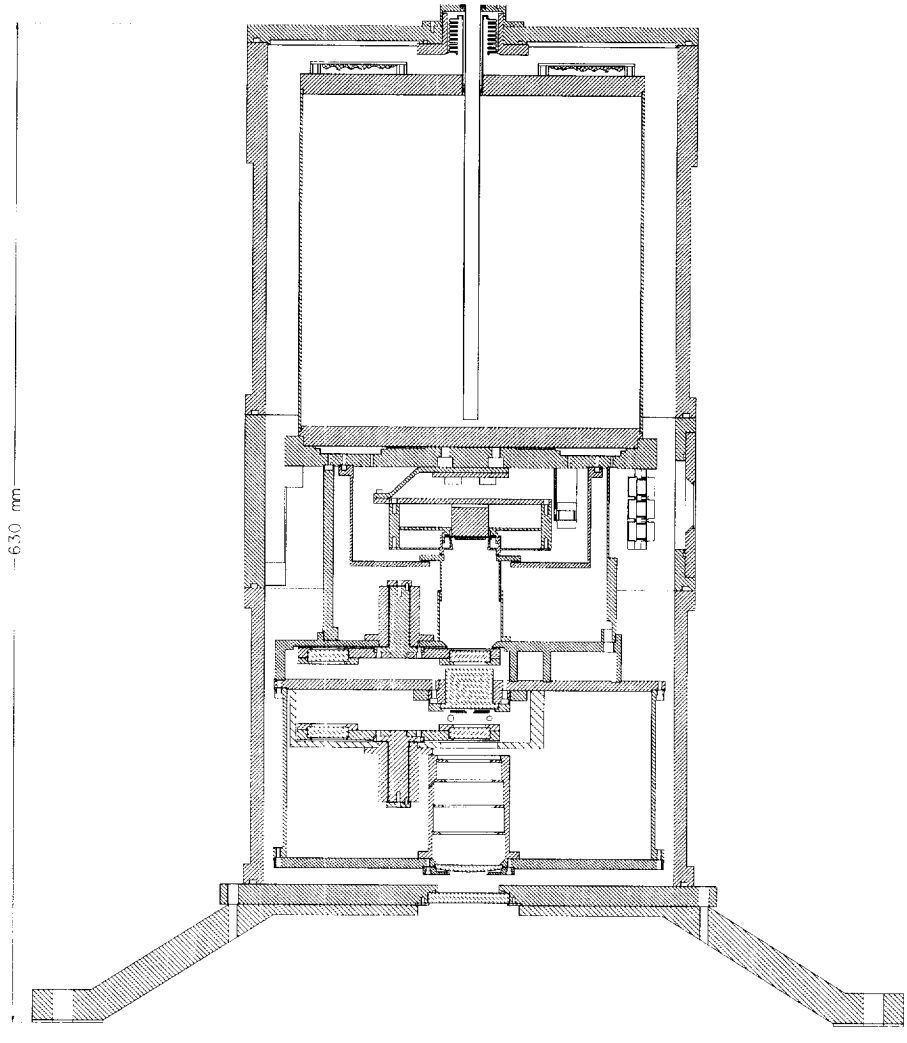

Fig. 2. Cross-section of QUIRC.

array was installed in QUIRC. Fig. 5 shows the flat-field response of this science-grade device. Fig. 6 shows a typical science frame, taken with the same observing parameters as Fig. 4, and scaled the same way as Fig. 4. Since the new detector array is mounted on a thicker substrate, the pixel scale of QUIRC has changed slightly to 0.188″/pixel. The new detector array is now in better thermal contact with the cryogen and is actively stabilized to an operating temperature of 80 K.

Fig. 7 shows linearity measurements of QUIRC with the science-grade HAWAII device, obtained by varying the shutter-limited integration time in dome flat-field exposures.

4. KSPEC

The cross-dispersed near-infrared spectrograph KSPEC (Hodapp, 1994), originally designed for a

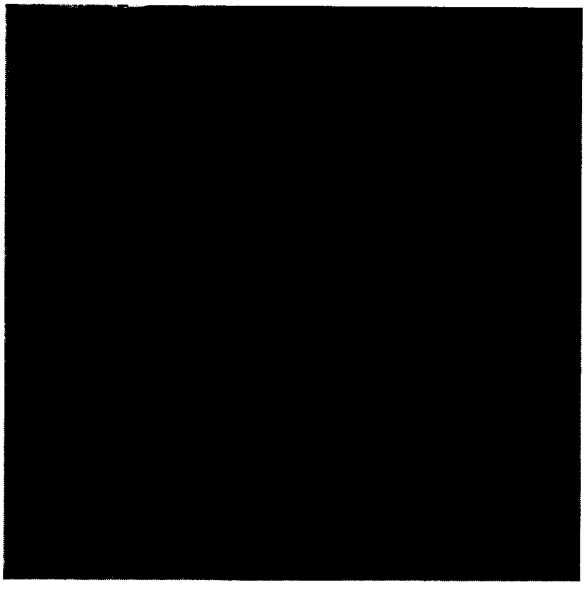

Fig. 3. H-band dome flat-field of QUIRC with the engineering-grade array.

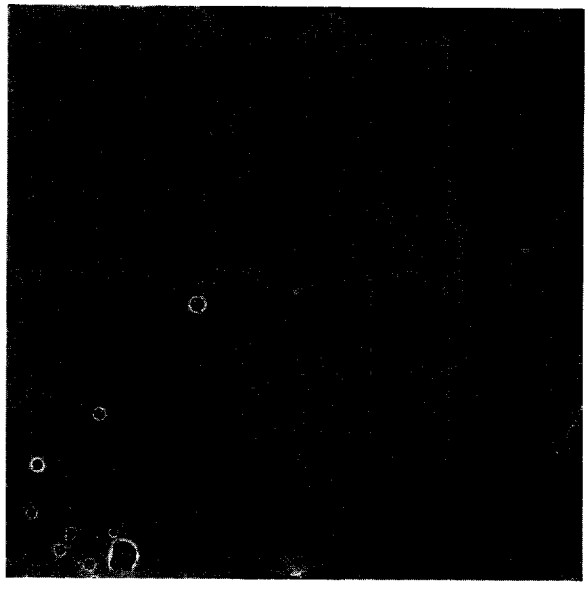

Fig. 4. Raw data frame of typical scientific observations taken with the first-generation engineering-grade HAWAII array in QUIRC. The frame is a 300 s exposure through the S(1) 2.12 μm filter, taken at the f/10 focus of the UH 2.2 m telescope at a pixel scale of 0.185″/pixel with QUIRC. The object is a field in L1634. For a comparison with Fig. 6, this frame is scaled in 1 e^- per data unit.

256 × 256 NICMOS-3 detector array, was upgraded for use with a 1024 × 1024 HAWAII array and used as a testbed for low-background operation of those devices. In the course of this upgrade, KSPEC was equipped with a spectrograph camera lens of longer focal length to illuminate the full format of the larger infrared array. In place of a folding mirror, an additional 34.5° ZnSe prism was added to the cross-disperser. Together with the existing 60° fused Silica prism, it gives about 90° beam deviation. With the HAWAII detector array, this new optical system achieves much finer spatial and spectral sampling than the original system. Thanks to the increased cross-dispersion, a longer slit (15″) can be used, allowing better sky subtraction. The slit-viewing camera was equipped with a science-grade NICMOS-3 detector array for better image quality.

KSPEC is intended to be used with the tip-tilt system at the f/31 focus of the UH 2.2 m telescope, which is now in common-user operation. The slit-width for the initial tests of KSPEC in the lab and at the telescope was 0.6″, with 0.2″/pixel spatial sampling on the HAWAII array. For projects requiring wider slits, such slits can be installed prior to an observing run.

The HAWAII array used in KSPEC is a second-generation engineering-grade device. The basic multiplexer design and detector technology are the same, but the fabrication technology, in particular the hybridization process, has progressed significantly in the year between the delivery of the two generations of devices. Cosmetically, this array is substantially better than the first engineering grade device originally used in QUIRC. The reason why it is not a full science-grade device is an area of higher-than-specified dark current in quadrants 3 and 4, a result of a problem in the HgCdTe material growth process. At an operating temperature of 72 K that we use at the telescope, achieved by pumping on the nitrogen in KSPEC's inner can, the dark current is

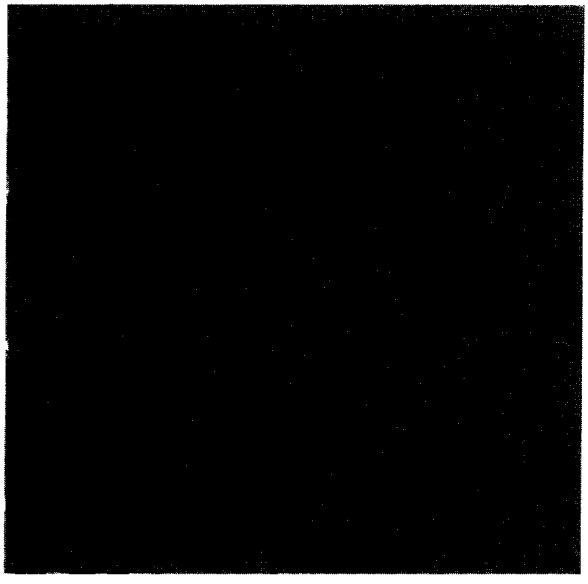

Fig. 5. H-band dome flat-field of QUIRC with the science-grade array. Compared to Fig. 3, the better uniformity and much smaller number of bad pixels is obvious.

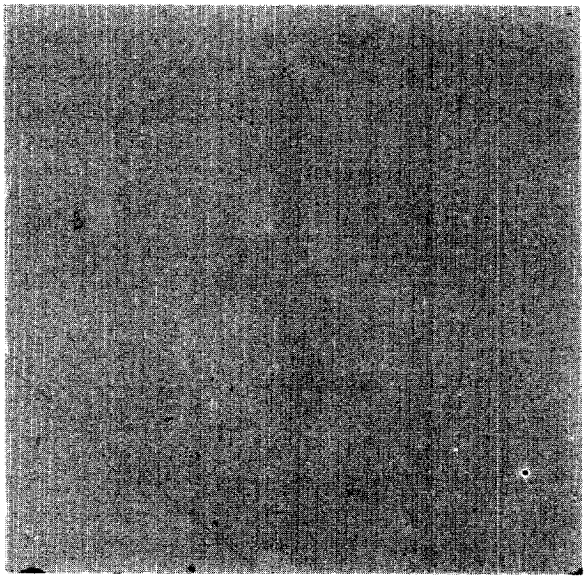

Fig. 6. Raw data frame of typical scientific observations taken with the science-grade HAWAII array in QUIRC. The frame is a 300 s exposure through the S(1) 2.12 μm filter taken at the f/10 focus of the UH 2.2 m telescope at a pixel scale of 0.188″/pixel with QUIRC. The object is a field in L1527.

low enough to allow scientific observations. Fig. 8, a typical raw data frame shows a faint, very red, slightly extended object.

5. The detector readout electronics

The HAWAII arrays are operated by a newly designed controller system intended to combine the best features of our older controllers with the more flexible device operation allowed by a DSP-based system. The digital portion is based on the **CCD controller developed by Leach**[20] (Leach, 1988).

We decided not to use the analog input and D/A pulse shaping capabilities of Leach's system, but rather to optically decouple digital clocking and data processing from any analog signal going in and coming out of the infrared array. For that, we developed a digital interface board that resides on the Leach controller backplane and uses the same addresses as the Leach analog board for the output of A/D values onto the backplane. Some of the addresses used by Leach to control D/A converters for pulse shaping are used to control the clocks. All signals are transmitted to the device drivers and received from the A/D board through optocouplers.

The device driver board switches between two constant but manually adjustable voltage levels. It allows read back of all of the voltages applied to the device through one of the A/D converters for the purpose of documenting instrument status and remote diagnosis of problems. The analog signal from the devices is preamplified, shifted by manually adjustable offset voltages, and sampled by 1 MHz Analogic A/D converters. The new data acquisition system now used for both QUIRC and KSPEC has a full signal chain, including A/D converter, for each of the four quadrants of the HAWAII device.

The 56000 DSP in the Leach system is not used

[20] http://mintaka.sdsu.edu/ccdlab

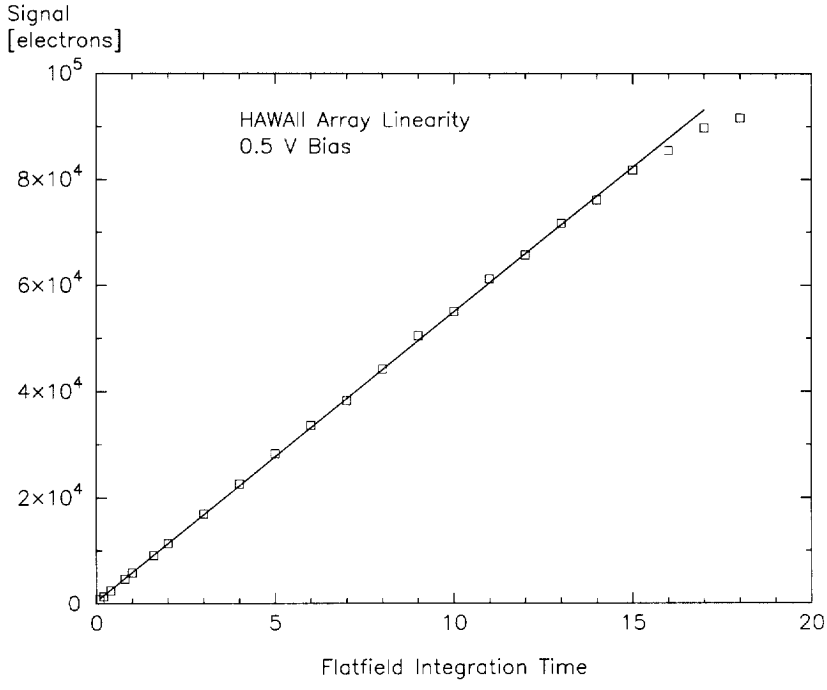

Fig. 7. Linearity measurements of the science-grade HAWAII array in QUIRC.

for signal processing due to the limited memory available on that DSP board. All raw data values are transmitted to the host computer (a SPARC LX or SPARC 2) via fiber optics, a fiber optics interface system, and an S-bus interface card, and are processed there. The data-processing requirements for the long integration times typically used with the HAWAII arrays are not very demanding, so this arrangement for data transmission and processing is adequate.

The multiplexer's four signal buses are each connected to the gate of an on-chip FET (see Fig. 1) that acts as a source-follower circuit to boost signal drive capability. Usually the FET's drain is connected to ground, and its source is connected to +5 volts (nominal) through an external load resistor. The horizontal bus is biased by an on-chip FET that serves as a constant-current generator.

It was believed, and later proven (see Section 7.1), that much of the glow observed in HAWAII arrays originates in the on-chip output FETs. To eliminate this source of glow, we used external p-channel junction FETs (JFET) connected directly to the bus, bypassing the on-chip FETs. In addition, we eliminated the current generator FETs and provided current to the bus using external 200 kΩ resistors connected to +5 volts. The on-chip output FETs' drain and source, and the on-chip constant-current generator gate and source were all left floating.

A p-channel JFET with a small pinch-off voltage was used because it provided the best match to the DC polarity and dynamic range requirements of the multiplexer's output bus and offered sufficient speed to accommodate the array's required read-out rate. The JFET selected was the Siliconix Inc. J270. This JFET performs well at 70 K; it has only a 0.4 V drop between its gate and source, at the desired bias-point (drain current of 0.5 mA nominal). This nominally matches the on-chip output FET DC bias parameters and allows a common pre-amplifier design for both

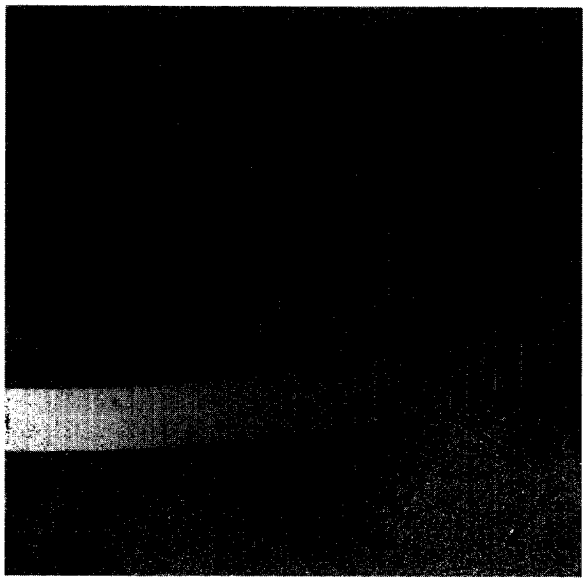

Fig. 8. Raw spectrum frame of a faint, slightly extended, very red continuum source obtained with KSPEC using the second-generation engineering-grade array. The lowest order is the K band, the second lowest is the H band, the shortest wavelengths recorded in the spectrum are around 0.85 μm.

modes of operation. The drain is connected to ground, and the source is connected to +5 volts through a load resistor. In addition, the J270 has good source-follower gain, about 0.968, and is reasonably linear. The linearity error, over an output range of several volts, is less than 0.6%. Also, the J270 offers a low output impedance, about 350 Ω, and introduces no significant noise into the system.

6. Detector performance for imaging

The first-generation HAWAII engineering-grade device used in QUIRC from July 1994 to December 1995 performed very well. QUIRC has not allowed us to fully verify the dark current performance of the array. The closest approximation to a dark current value are exposures through the J filter against an ambient temperature surface. Those data indicate a dark current of ≤ 1.0 e^-/s on average, with substantial spatial variations. The same array, when tested in a dewar better suited for that purpose at Rockwell, and operating at 77 K, achieved dark currents of < 0.1 e^-/s.

The quantum efficiency of that first engineering array left some room for improvements. We measured about 42% in K, 45% in H, and 27% in J. Very similar values have been measured on NICMOS-3 devices at the same telescope (Hodapp et al., 1992).

The new science-grade array has a much lower number of bad pixels, and a certain class of single-pixel defects leading to "doughnuts" of higher dark current (Fig. 4) are absent in that new device. These defects were caused by a processing problem in the multiplexer fabrication that has now been identified and resolved. The quantum efficiencies of the science-grade HAWAII array at an operating temperature of 80 K are: J: 39%, H: 57%, K: 53%.

When operated at the same elevated temperature as the original engineering-grade array (96 K), the science-grade device showed unacceptably high dark currents. At 80 K, the dark current is sufficiently low to be smaller than the sky backgrounds in all filters, but since we do not have a blank-off position in the filter wheel or pupil slide, we cannot give a precise value for the dark currents of devices tested only in QUIRC. For the science-grade array, exposures through the J filter against an ambient temperature surface indicate an average dark current of ≤ 0.8 e^-/s.

For a comparison of the overall quality of the raw data, Fig. 4 shows a raw frame, with data scaled to electrons, of a 300 s exposure in the S(1) 2.12 μm filter at the f/10 focus of the 2.2 m telescope using the HAWAII engineering-grade device. Fig. 6 is a raw frame, again scaled to electrons, taken with the science-grade device, with the same exposure parameters. The higher cosmetic quality of the science-grade array is obvious from this comparison.

7. Low-background tests in KSPEC

7.1. Introduction

The HAWAII arrays were designed for use in

high-resolution near-infrared spectrographs. The sky brightness in the near-infrared is dominated by a relatively small number of discrete emission lines, mostly from OH (Maihara et al., 1993). In between the OH airglow lines, the sky brightness reaches the minimum between zodiacal light scattering and thermal emission somewhere in the H band.

It has been demonstrated that this window can be exploited using OH suppression spectrographs that mask off the OH lines in a high resolution spectrum before recombining the light into a low resolution spectrum or a slit image (Iwamuro et al., 1994). The simpler approach of directly recording the high-resolution spectrum and to digitally combine only those spectral elements that are unaffected by OH lines puts extreme demands on the detector arrays. The design of the HAWAII arrays intended to come as close as current technology allows to meeting this requirement.

7.2. Fringing

KSPEC flatfield exposures (Fig. 9), as well as all raw data of stars, clearly show interference effects in the sapphire substrate on which the HgCdTe detector material is grown. This interference leads to a modulation of the spectrum with a peak-to-valley variation of 10% of the signal value.

This interference effect in the sapphire is very stable with time. The problem for the use of the spectrograph is that it is practically impossible to illuminate the slit in the same way for objects as for flatfields, and that even between objects and standards, the illumination through the slit may vary substantially. In KSPEC the spacing of these interference fringes (≈ 9 pixels in K) is of the same order as the slit width (usually 5 pixels for 1″ slits). KSPEC is normally used at the f/31 focus with fast tip-tilt correction, where diffraction-limited image quality can be achieved. Unfortunately, the guider system flexes relative to the science beam on time-scales of several minutes by a fraction of an arcsecond, so that the use of a diffraction limited slit (e.g., 0.2″) for stellar work is very difficult. Also, KSPEC has a fixed slit that can only be exchanged when the instrument is opened. To accommodate observations of extended objects, the compromise is to use slits of $\approx 1''$ in width. For point sources, the object significantly underfills the slit and the illumination is very non-uniform across the slit, leading to imperfect flatfielding of the interference pattern.

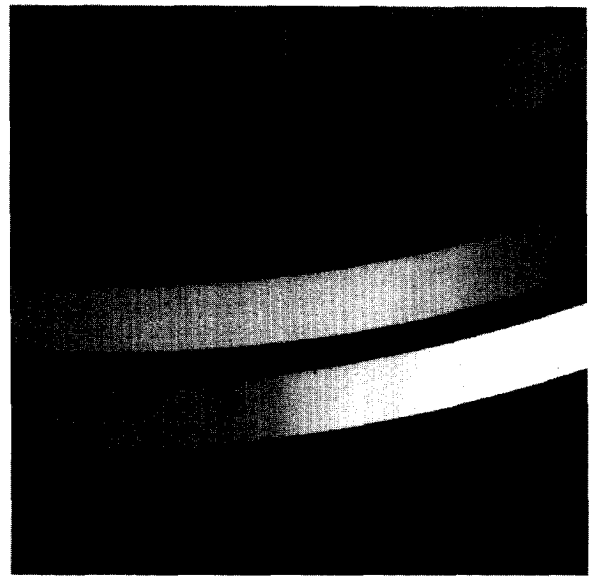

Fig. 9. Interference effects in a KSPEC flat-field frame. The interference is caused by the sapphire substrate on which the HgCdTe is grown.

7.3. Amplifier glow

The HAWAII multiplexer has several sources of electroluminescence. The most important of these is the photon emission from the output source follower FET. The multiplexer was designed so that these output FETs on the multiplexer can be bypassed (Fig. 1). Using external JFETs to amplify the bus signal reduced the glow associated with the outputs by about a factor of 5. Compare Fig. 10, glow-test-1548 (internal FETs) with Fig. 11 (glow-test-611, external FETs), both taken with $n_{\mathrm{sample}} = 16$, and the same operating voltages for the multiplexer. Even with external FETs and an external 200 kΩ resistor

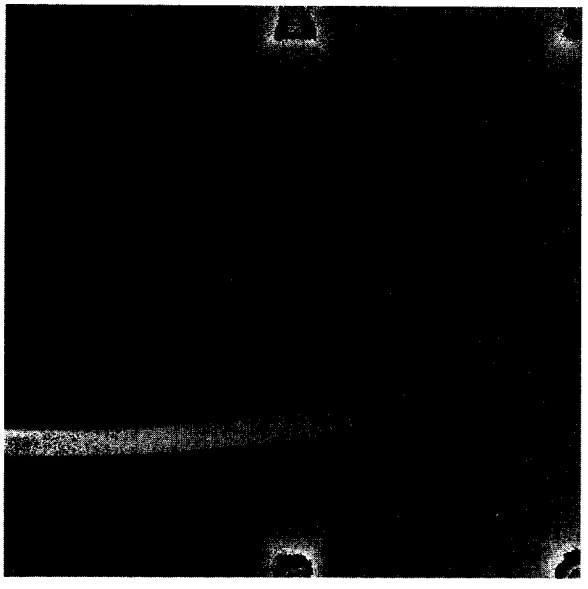

Fig. 10. Multiplexer glow tests: All multiplexer operating voltages at 5.0 V, 16 samples, internal multiplexer output FETs used. Using the internal FETs increases the electroluminescence at the location of the output amplifiers by about a factor of five compared to using external FETs (as in Fig. 12).

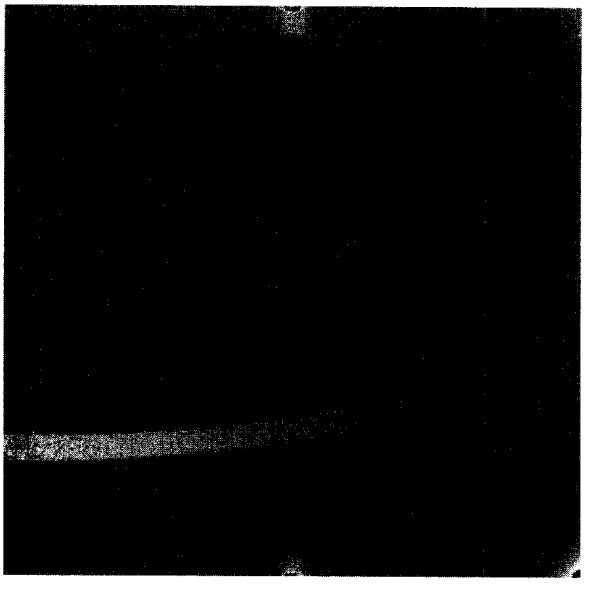

Fig. 11. Multiplexer glow tests: Nominal setting of the multiplexer operating voltages; V_{dd} = 5.0 V, clock-high = 5.0 V. For this test, the external JFETs were used.

to set the bus current, some glow is still visible near the output area of the multiplexer. The source of this glow is a clock driver circuit in the shift register. It cannot be eliminated without a redesign of the multiplexer.

As with the NICMOS-3 devices, the glow is proportional to the number of reads of the device and not to the integration time. For long integration times and CDS reads, glow effects are therefore negligible. For multi-sampled exposures the glow effects are prominent, but even then they only affect a relatively small area of the device.

When using the external JFETs, the remaining glow can be minimized by setting the voltage V_{dd} to less than the 5.0 V nominally used. We achieved minimal glow at $V_{dd} = 4.2$ V (Fig. 12, frame glow-test-607), compared to Fig. 11 (frame glow-test-611) with all multiplexer voltages set to 5 V. Still lower voltages, as in Fig. 13 (frame glow-test-605) (V_{dd} = 4.0 V) lead to massive shift register glow.

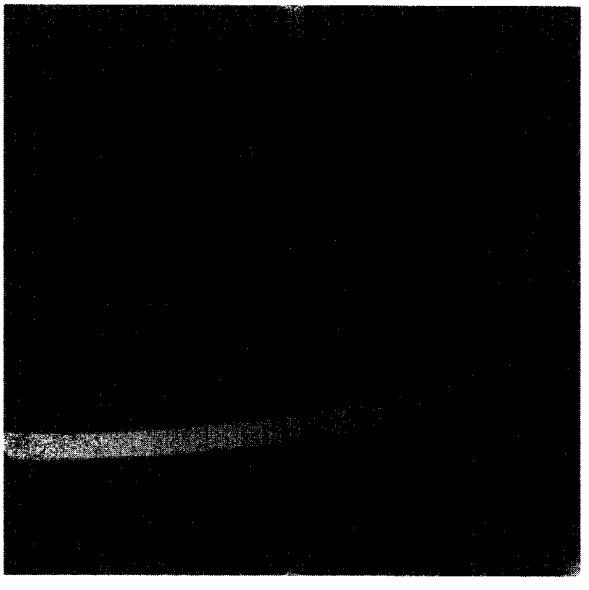

Fig. 12. Multiplexer glow tests: Optimal setting of the multiplexer operating voltages; V_{dd} = 4.2 V, clock-high = 5.0 V. For this test, the external JFETs were used.

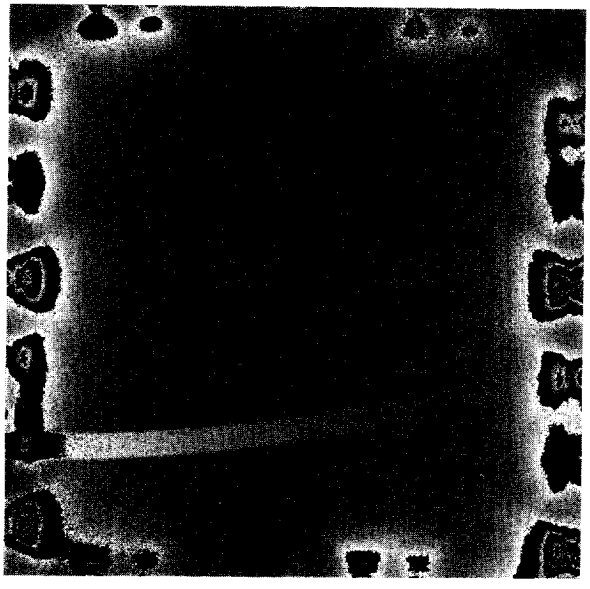

Fig. 13. Multiplexer glow tests: $V_{dd} = 4.0$ V, clock-high = 5.0 V. Setting V_{dd} too low leads to massive glow of several multiplexer components.

7.4. Noise and dark current

The tests of low noise and low dark current performance in KSPEC were done with a first-generation prototype device that, aside from the problem of hybrid reliability, showed very good performance. Over the course of the tests in KSPEC, this device deteriorated with each thermocycle and developed more and more bad pixels. However, the performance of the pixels that stayed connected was not affected by this slow delamination of the device and their performance is characteristic of the second-generation devices produced with better hybridization technology.

The gain of the data acquisition system was calibrated using the usual method of measuring the shot noise in high-signal exposures. In long integration times, computing the noise for individual pixels from a sequence of frames taken under identical conditions is not a viable method. Drifts in the signal chain electronics and in the flux level of the illuminating light source will cause significant, if not dominant, noise contributions that are unrelated to the quantum nature of the detected photon flux. Therefore, such noise measurements are not suited for gain calibration. Instead, pairs of CDS exposures taken under identical conditions were subtracted, and the standard deviation of subsets of pixels in the difference frames was computed and then divided by $\sqrt{2}$ so that the noise refers to a single CDS exposure. Individual bad pixels were marked and excluded from the computation of the statistics. Since KSPEC illuminates only a fraction of the array, a number of subframes in the K band were defined with approximately uniform illumination, plus some adjacent unexposed areas to monitor signal drifts in the detector. The average of the signals measured in those unexposed areas was subtracted from the signal measurements in the K window, so that only true signal due to photons enters the gain calculation, and contributions from electronics drifts are eliminated.

The gain of our data acquisition system was designed to be 6.63 μV/ADU. For the tests discussed here, a software scaling factor of 2 was used so that the effective gain was 13.3 μV/data-unit. Using the value of 0.78 for the total source follower gain given by (Kozlowski et al. (1994)), our gain measurements in KSPEC give integrating node capacities of 43.2 fF at 100 mV bias and 42.2 fF at 250 mV bias. Similar calibration measurements at 500 mV bias in QUIRC gave 34.7 fF capacitance, compared to 36.6 measured at the same bias on a different device by Rockwell. For higher detector bias, the integrating node capacitance is lower. (Kozlowski et al. (1994)) give values around 20 fF for a detector bias of 1.0 V.

For measurements under the lowest background conditions, the optical path of KSPEC was blocked to avoid stray light. To reduce the effective read-noise to minimal levels, multiple non-destructive reads of the device were used (Fowler & Gatley, 1991). With the detector array operating at about 65 K, we took a series of integrations using multiple, non-destructive reads to reduce the noise, while keeping the time from the beginning of the first read to the beginning of the last read constant. We then varied the number of reads at the beginning and the

end of the integration time in increments of factors of 2, from 1 (CDS) to 128. With 128 samples taken at the beginning of the integration time and 128 at the end, a 600 s total exposure time was almost completely filled with reads of the device. Fig. 14 is a 3600 s total integration time, $n_{\text{sample}} = 128$ frame at 65 K operating temperature and 100 mV detector bias.

The results of low background, long-integration time noise tests with 600 s and 3600 s total exposure time are shown in Figs. 15 and 16. They differ in the detector bias setting. We used detector bias levels of 250 mV (Fig. 15) and 100 mV (Fig. 16) for these tests. At these low bias values, the full-well capacity of the device is small ($\approx 20\,000$ e$^-$), but for low-signal applications in a high-resolution spectrograph, for example, this is an acceptable price for lower dark current.

We found it impractical to measure dark currents of the order of 1 e$^-$/min directly by the accumulated signal in long integration times. During integration

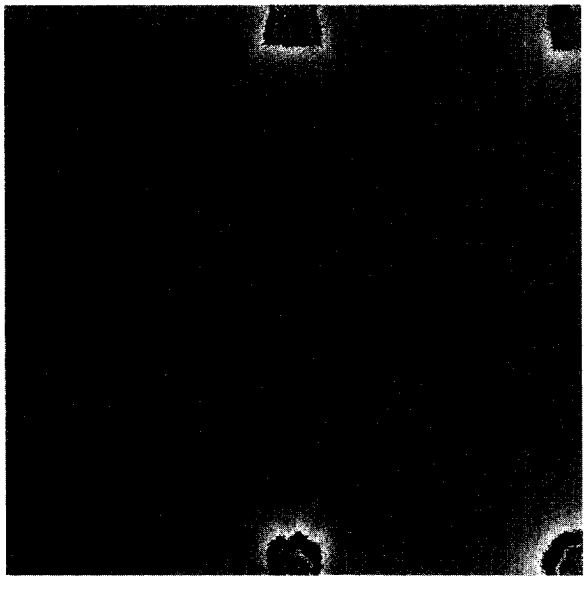

Fig. 14. Multi-sampled dark current data: 65 K operating temperature, 128 samples, 3600 s total integration, external JFETs used. For this frame, the optical path of KSPEC was blocked by a cold blank so that no thermal radiation is seen in the K band.

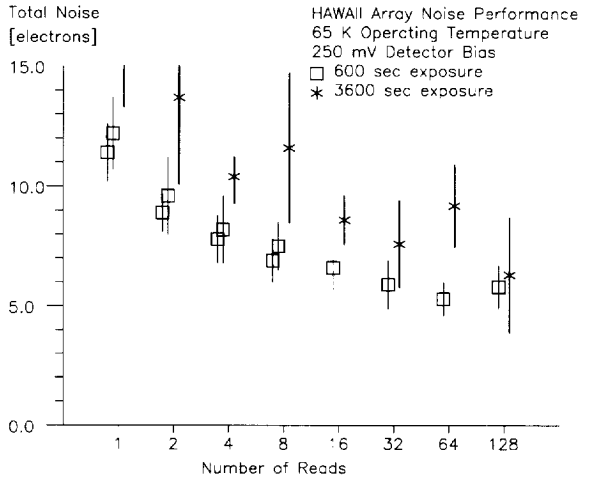

Fig. 15. The total noise measured under low-background conditions, at 65 K operating temperature and 250 mV bias settings, depends on the number of non-destructive reads taken at the beginning and at the end of the integration time. The integration time is the time from the beginning of the first read to the beginning of the last read, irrespective of the number of reads. The noise is the total noise accumulated, divided by the number of reads.

times of one hour, signal drifts caused by instabilities in the electronics and thermal drifts in the cryostat produced random signal shifts approximately equal to the expected dark current. These drifts tend to be larger in longer integration times, i.e., they have approximately 1/f characteristics. An upper limit to the integration time was set by the periodic refills of liquid nitrogen and the thermal instabilities associated with this procedure. While a direct measurement of the dark current is certainly desirable for understanding the detector material, a measurement of the shot noise associated with the accumulated dark current is more relevant for astronomical applications. This noise increase is not necessarily only due to true detector dark current, but also due to photon leaks in the instrument or 1/f effects in the unit cells. In any case, the increased noise due to any of the above effects is more relevant for the astronomical performance than the question of what the true dark current is.

Our data indicate that for correlated double sam-

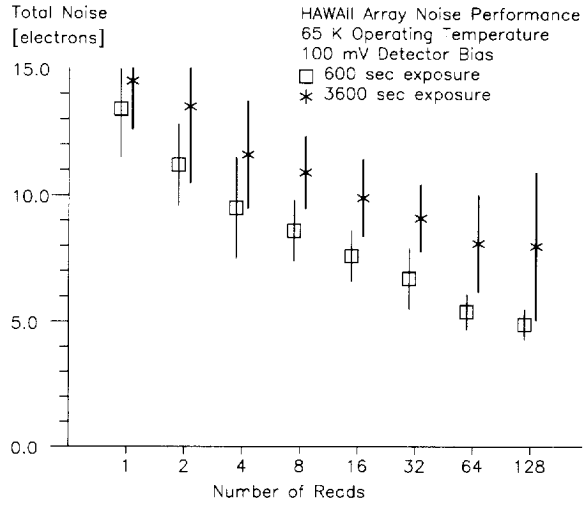

Fig. 16. The total noise measured under low-background conditions, at 65 K operating temperature and 100 mV bias settings, depends on the number of non-destructive reads taken at the beginning and at the end of the integration time. The integration time is the time from the beginning of the first read to the beginning of the last read, irrespective of the number of reads. The noise is the total noise accumulated, divided by the number of reads.

pling (CDS) reads ($n_{\text{sample}} = 1$), the noise in long integration times is between 10 and 15 e^- rms. Multi-sampling reduces the noise. In 600 s and with 128 samples (i.e., 128 in the beginning, 128 at the end of the integration time, and the signal being the difference of the last 128 frames minus the first 128 frames), the noise is reduced to about 5 e^- rms. This value is the total measured noise, divided by 128, but does not take into account the shorter mean photon collection time per sample pair in a situation where the whole available integration time is filled with reads. For 3600 s integration time, the noise in multi-sampling begins to level off at about 8 e^- rms at 64 reads, indicating that shot-noise contributions are dominating the total noise at this number of reads. These noise numbers are an average of many individual noise values obtained in different frame pairs, and on different locations on the array. The error bars in Figs. 15 and 16 indicate the rms scatter of those individual noise measurements. Quadratic subtraction of the pure readnoise from the total noise leaves a noise component due to dark current corresponding to 39 accumulated electrons in 3000 sec, or 0.8 e^-/min. The 1σ upper limit to the total noise corresponds to 2 e^-/min, the lower limit formally corresponds to zero dark current. Given the uncertainties of the noise measurements and the fact that noise source other than dark current shot noise may contribute, the best way to summarize the results is that with $n_{\text{sample}} = 128$, and with integration times much longer than 600 s, e.g., 3600 s, the readnoise is below 5 e^- rms and the dark current is below 1 e^-/min at an operating temperature of 65 K. At these levels of performance, HAWAII detectors are very well suited for high resolution near-infrared spectroscopy, where extremely low background levels are achieved between the OH airglow lines.

7.5. Residual excess dark current

The residual excess dark current effect, the fact that pixels previously exposed to radiation show an increased dark current in subsequent exposures, has been characteristic of NICMOS-3 devices. We conducted several tests with the HAWAII arrays to determine to what degree this problem persists. Since the methods used for growing HgCdTe material and for implanting diodes into the HgCdTe have not changed much since the NICMOS-3 production, we expected that the residual excess dark current problem would still be present in the new HAWAII arrays.

An extensive series of tests was done to measure the excess dark current of pixels previously exposed to high flux levels. The tests were carried out using KSPEC, and the bright illumination was provided by an Argon lamp that has spectral lines of a wide range of intensities in the near infrared. After an initial 20 s exposure to the Argon lamp, the instrument shutter was closed off and subsequent 100 s integrations were taken against the ambient temperature shutter. Two series of tests were done. In the first, we compared the residual excess dark current level under the following operating conditions:

- Reset line pulsed on once per line during the reset frame prior to the CDS dark frames, i.e., normal operation of the reset for line-by-line resetting.
- Reset line pulsed 50 times per line during the reset frame, i.e., while any given line of the device was addressed for resetting, the reset line was pulsed 50 times.

Pulsing the reset line 50 times did not lower the residual dark current substantially. Fig. 17 compares the decay of the residual excess dark current for a number of subframes exposed to different levels of flux in the initial Argon frame.

In a second test, we compared the normal read-out mode with a single reset frame (single pulse per line) prior to a CDS pair to a mode where a double-correlated exposure is preceded by 100 reset frames, each with the reset line pulsed once. Fig. 18 shows the results of this comparison. The additional reset frames obviously help in reducing the residual excess dark current by more than a factor of two. This gain has to be traded off against the additional time required for the large number of reset frames.

In addition, we have additional clocking schemes that had the potential for erasing the residual excess dark current. We tried applying a high detector bias prior to the normal integration, applying a zero bias to the detector prior to the normal readout sequence, etc. While some of these tricks do erase previous residual image information, they usually cause different, but equally ugly, latent effects. Turning the power to the system off for a few minutes does erase

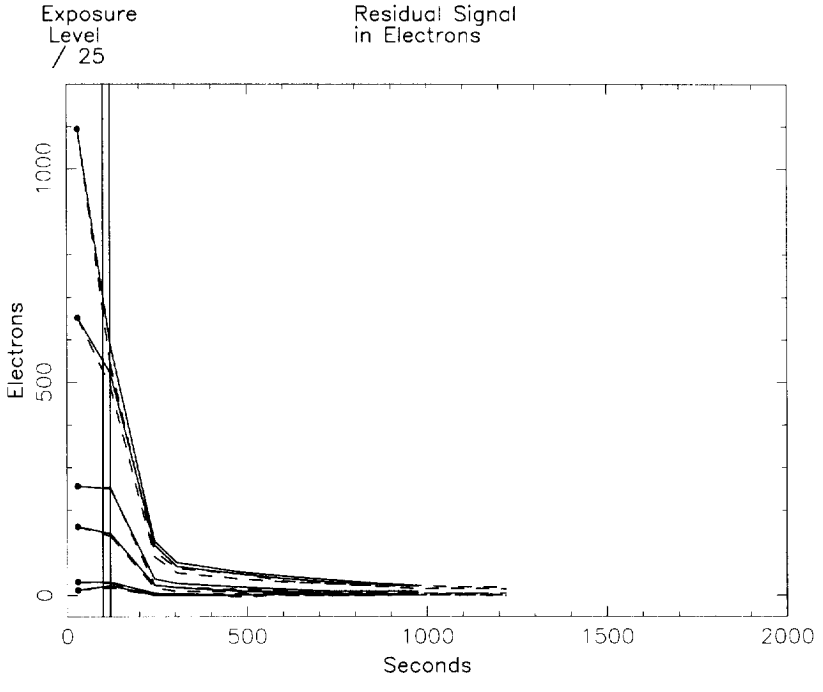

Fig. 17. Residual image effects. The first data point, near the zero point of the time axis, represents the flux level in the bright exposure that preceded the dark current measurements. To fit on the same signal scale, this value is scaled by a factor 1/25. To the right of the vertical double dividing line, dark current values are plotted. Dashed lines represent frames with normal reset, solid lines represent frames reset by multiple switching of the reset line. The residual excess dark current from a previous, bright exposure of the detector array is not significantly reduced by pulsing the reset switch repeatedly (50 times).

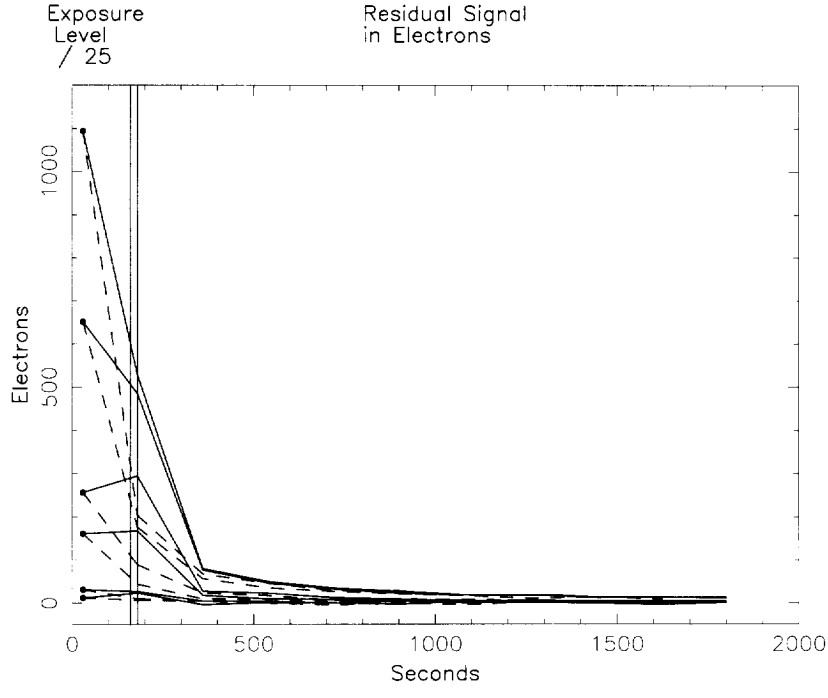

Fig. 18. Residual image effects. The first data point, near the zero point of the time axis, represents the flux level in the bright exposure that preceded the dark current measurements. To fit on the same signal scale, this value is scaled by a factor 1/25. To the right of the double dividing line, dark current values are plotted. Solid lines represent data with one reset per frame, dashed lines are frames preceded by 100 reset frames. The residual excess dark current from a previous, bright exposure of the detector array is somewhat reduced by resetting the device 100 times with full reset frames.

the residuals but leaves the system too unstable to continue with long, high-sensitivity integrations immediately after powering up again.

Consequently, in low-background observations, care should be taken to avoid saturating the detectors. Accidentally saturated pixels will show a residual image that decays on a timescale of a few minutes.

Direct imaging is somewhat less affected by the residual excess dark current; background levels are generally higher than in spectroscopy, so that small excess dark current is not significant. Images taken with QUIRC through a narrow-band filter at 2.12 μm, i.e., under relatively low-background conditions, did not leave a detectable residual image up to about 40% of full-well exposure level in the preceding exposure.

8. Fast sub-array reading for wavefront sensing

Wavefront sensing in the infrared has a number of advantages over the use of shorter wavelengths for that purpose (Gillett, 1995). For most stars, the photon flux peaks at near-infrared wavelengths, the seeing is better in the infrared, and even in obscured regions of the sky, guide stars will be available in the infrared. A disadvantage is the higher sky background at longer wavelengths, due to more intense OH airglow and thermal emission.

Up to now, however, the performance of near-infrared detector arrays was not good enough for infrared wavefront sensors to be competitive with fast-reading optical CCDs or avalanche photodiode systems. The low noise, low dark current, and good quantum efficiency made it likely that HAWAII

arrays could achieve a performance level adequate for low-order wavefront sensing for the Gemini near-infrared instruments. In the following sub-sections, we describe our tests of HAWAII arrays in fast sub-array operation. The QUIRC camera with the science-grade array was used for these tests.

8.1. Description of experiment

We decided to read a sub-array of 8×8 pixels to simulate the data acquisition for a 2×2 Shack-Hartmann sensor with each spot position measured by a quad cell and the surrounding pixels used for sky measurements.

The two shift registers in the HAWAII array were found to operate at different speeds. The line clock, clocking in vertical direction (in our usual display orientation for images) from one (horizontal) line (512 pixels) to the next, needs at least 250 ns per step to operate properly. We chose to operate this clock at a safe 1 μs. The column clock, addressing columns by clocking horizontally, operates more slowly, at maximum speed of 1.5 μs. We chose to operate this clock at 3.0 μs.

The tests were conducted using external JFET amplifiers connected to the multiplexer bus, bypassing the on-chip FETs to avoid the glow associated with operating them.

8.2. Selection of quadrant and sub-array location

The sub-array location that can be addressed fastest is at the beginning of both the line and the pixel shift registers. For two of the four quadrants, this position is affected by glow from the output amplifiers and shift registers. It is therefore useful to locate the sub-array a few pixels away from the location of the quadrant output. For quadrants 3 and 4, the position of the amplifiers does not coincide with the starting point of the shift registers. For quadrant 4, in particular, the shift registers start in the center of the 1024×1024 array.

We chose the starting point of the sub-array to be 50 lines and 2 columns from the shift register starting point, a position that would be usable in all four quadrants. Our test were done in quadrant 4, i.e., near the center of the 1024×1024 device. Fig. 19 shows the bright star at the approximate location of the sub-array, in a full frame. The two bands of lower background level are those areas of the detector array that were continually reset during the fast sub-array operation. The other areas of the devices had saturated during those tests and are now showing a residual excess dark current.

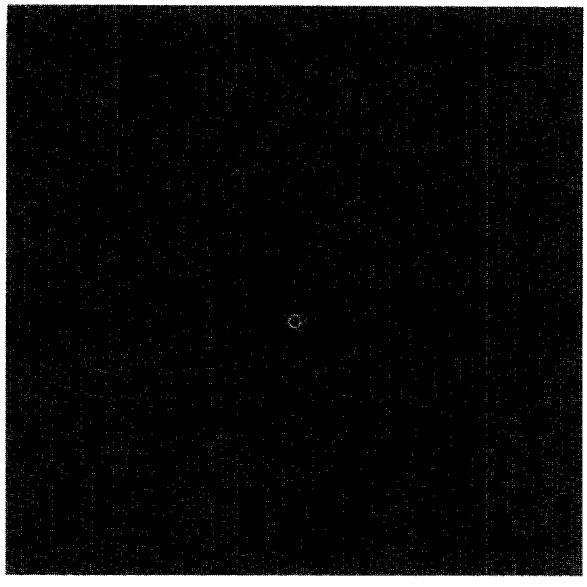

Fig. 19. The location of the sub-array for the fast read-out tests is indicated by the image of the bright star (taken under very bad seeing conditions). We reset the first 100 lines of each quadrant and left the rest of the array to saturate. As a result, those saturated pixels still show a residual excess dark current in this image.

8.3. Read-out speed and timing

We measured the noise in fast sub-array reads at two different clocking rates:

1. At 10 μs address time per pixel, similar to the clocking speed for our full-frame read-out mode. In this mode, and with the given values for the analog filtering, the time constants of our JFET booster FETs, and the slew rate of our preamp op-amps, the

analog signal has ample time to settle before A/D conversion begins 9 μs after the pixel was addressed. Given that the signal has ample time to settle, fixed pattern noise is substantially lower in this mode than in the faster mode described below. In the 10 μs per pixel mode, reading a single frame of 8×8 pixels takes 760 μs. The frame repeat time of 18 ms was chosen so that reading the sub-array 20 times for multi-sampling consumed all the available time (15.2 ms). The remaining 2.8 ms were used for resetting and other overhead.

2. At 5 μs address time per pixel. At this speed, the signal does not have time to settle to a DC value before A/D conversion starts. This read-out mode leads to significant fixed pattern effects, but white noise components are not noticeably higher than in the slower read-out mode. In this read-out mode, one read of the sub-array takes 440 μs, or 8.8 ms for 20 reads. The overhead for resetting is the same, the total frame repeat time is therefore 11.6 ms.

We did not modify the filtering or the output amplifier JFETs for the fast read-out tests. For this reason our tests are limited to a pixel read-out time of 5 μs. As demonstrated by (Kozlowski et al. (1994)), however, HAWAII arrays can be operated at pixel rates of 3 μs without noise penalty. The use of the external JFETs is not necessary for the fast read-out of small sub-arrays, since the output FET glow is proportional to the total number of pixels read through the amplifier in the process of reading a frame, and is consequently quite small for small sub-arrays, even with multiple sampling.

8.4. Noise and gain measurements

For measurements of the read-noise in fast sub-array reads, we defined the noise of a pixel as the standard deviation of the signal differences of two consecutive CDS frames, divided by $\sqrt{2}$ to give the noise in an individual CDS frame, rather than in the difference frames. This assumes that in the absence of noise, the difference of frames taken 11 or 18 ms apart is zero, i.e., that signal drifts are negligible on these timescales. Note that each of the two frames subtracted here is a full CDS frame. The gain (e^-/adu) is measured by assuming that the noise in high signal frames is pure shot noise of the signal collected. This definition of read-noise ignores noise components due to signal drifts. Since such noise components are related to the analog signal chain electronics rather than to the photon statistics of the signal, their inclusion would lead to an overestimate of the noise in high-signal frames and, consequently, an underestimate for the gain and the read-noise. Note that the definition of read-noise is different from that used for long integration times in the tests done with KSPEC. For integration times as long as 1 hour, signal drifts dominate over read-noise. For KSPEC, we measured the noise not as the temporal variation of the signal of an individual pixel, but as the pixel-to-pixel variation of sky-subtracted frames.

Since the capacitance of HgCdTe photodiodes is a function of the bias (Kozlowski et al., 1994), the gain was measured on signal levels well below the saturation of the device, but well above the square of the read-noise. For signal levels between 2000 e^- and 40000 e^-, the average gain of QUIRC at a detector bias of 0.5 V was 3.7 ± 0.2 e^-/adu.

For noise measurements in multi-sampled mode, the total time elapsed from the beginning of one frame to the start of the next frame (the frame repeat time) was kept constant. To compare the noise for different numbers of samples, one divides the total measured noise by the number of samples, but also has to correct for the shorter photon collection time per pair of reads.

For each of two read-out speeds, the first column in Table 1 gives the total measured noise in electrons (gain = 3.7). The second column is the noise scaled to the gain and photon collection time of the double-correlated read ($n_{\mathrm{sample}} = 1$). It is the number in the

Table 1
Multi-sampling noise measurements (e^-)

n-sample	10 μs reads		5 μs reads	
1	10.3	10.3	9.50	9.50
2	15.1	7.97	13.8	7.28
4	22.1	6.56	20.5	6.09
8	31.9	6.31	30.7	6.08
10	34.2	6.50	–	–

first column, multiplied by the scaling factor $((20 - 1)/(20 - n_{sample}))/n_{sample}$.

The best sensitivity is achieved by sampling the signal for about the first quarter of the integration time, not sampling in the second and third quarters of the integration time, and sampling again in the last quarter. Samples in the first quarter are subtracted and samples in the last quarter are added to form the final multi-sampled signal.

8.5. Operating temperature

In the lab, the device temperature was varied between 83 K and 109 K. A constant signal was produced by diffuse illumination of a screen by a blackbody radiation source. We found that up to the highest temperature tested, the fast sub-array operating mode worked. Only at the highest temperature did the dark current become the noise limiting factor; at 109.4 K, we measured a dark current of approximately 2400 e^-/s. At 105 K, the dark current was about 930 e^-/s; its shot-noise in 10 ms integration time is thus smaller than the read-noise. In earlier experiments done with KSPEC, we found that the HAWAII multiplexers do not operate well below 60 K. This limitation was deliberately accepted so that sub-micron CMOS procedures could be used in fabricating the multiplexers. Our experiments did not show a significant change in signal level between 85 K and 109 K, therefore there is little to gain in terms of quantum efficiency by operating at the higher temperature. We conclude that for the fast sub-array read-out mode, any operating temperature between 65 K and 100 K would be possible, with no significant performance difference within that range.

8.6. Possible improvements

Our tests simulated a realistic data acquisition system for a 2×2 Shack-Hartmann wavefront sensor. The results indicate that the HAWAII arrays operate well in fast sub-array read-out mode and that noise values of about 6 e^- rms are readily achieved with frame repeat times of 11 ms. This level of performance makes the HAWAII arrays well suited for the low-order wavefront sensing applications planned by Gemini.

Some improvements in the sensitivity are possible, however:

1. The read-out speed could be increased by about a factor of two. This requires optimizing the analog signal chain for higher speed operation. We expect that the trade-off between the number of reads possible in a given time and the wider filter bandwidth required favors the faster reads and the wider bandwidth, so that a net reduction in noise would result.

2. The role of the line and column shift registers should be reversed from what we used. Since the column clock cannot be operated as fast as the line clock, the columns should be clocked as infrequently as possible.

3. The location of the sub-array could be optimized to minimize the pixel addressing times.

4. A smaller number of lines could be reset.

We assumed that the four Hartmann spots are recorded in a contiguous set of 8×8 pixels. A more efficient way of reading out would be to place the four spots into the equivalent locations in the four quadrants of the array. In this case, the four quadrants would be clocked simultaneously and read out through four independent signal chains. The disadvantage is that this requires a device of higher quality, with all four quadrants functional and defect-free spots in the same location of the four quadrants. Also, the relative location of the four spots must precisely match the separation of the quadrants, a requirement that may be hard to meet. In our judgement, the potential noise reduction possible with this method is not worth the added cost and complexity of the system.

For fast reads, fixed-pattern noise is present in the images, and this fixed pattern increases proportional to the number of reads. The data acquisition system must therefore be capable of subtracting a fixed pattern in real time. In our tests, we found the fixed pattern to be stable on timescales of a few hours. Still, occasional recalibration may be required.

Acknowledgments

The development and testing of the HAWAII arrays was supported by the State of Hawaii and NASA grant NAGW-3643, with funding from the Air Force Phillips Laboratory. Testing of HAWAII arrays for wavefront sensing was supported by the Gemini 8-m Telescope Project, which is managed by the Association of Universities for Research in Astronomy, for the National Science Foundation, under an international partnership agreement.

References

Fowler, A.M. & Gatley, I., 1991, in: SPIE Infrared Sensors: Detectors, Electronics, and Signal Processing, p. 1541.

Gillett, F., 1995, Gemini Technical Report TN-PS-G0031.

Hodapp, K.-W., Rayner, J., & Irwin, E., 1992, PASP, 104, 441.

Hodapp, K.-W., Hora, J.L., & Irwin, E., 1994, PASP, 106, 87.

Hodapp, K.-W. & Ladd, E.F., 1995, ApJ, 453, 715.

Iwamuro, F., Maihara, T., Oya, S., Tsukamoto, H., Hall, D.N.B., Cowie, L.L., Tokunaga, A.T., & Pickles, A.J., 1994, PASJ, 46, 515.

Kozlowski, L.J., Vural, K., Cabelli, S.A., Chen, C.Y., Cooper, D.E., Bostrup, G.L., Stephenson, D.M., McLevige, W.L., Bailey, R.B., Hodapp, K., Hall, D., & Kleinhans, W.E., 1994, Proc. SPIE 2268, 353.

Leach, R.W., 1988, PASP, 100, 1287.

Luppino, G.A. & Miller, D.R., 1992, PASP, 104, 215.

Maihara, T., Iwamuro, F., Yamashita, T., Hall, D.N.B., Cowie, L.L., Tokunaga, A.T., & Pickles, A., 1993, PASP, 105, 940.

Roddier, F.J., Anuskiewicz, J., Graves, J.E., Northcott, M.J., & Roddier, C.A., 1994, in: Adaptive Optics in Astronomy, eds. M.A. Ealey and F. Merkle, Proc. SPIE 2201, 2.

Thompson, R.I., 1994, in: Infrared Astronomy with Arrays: The Next Generation, ed. I.S. McLean, Kluwer, p. 253.